

A Bioinspired Hierarchical Underwater Superoleophobic Surface with Reversible pH Response

Xia Huang, Hatice Mutlu, and Patrick Theato*

The development of oil-repellent surfaces in liquid environments has received considerable attention because of the urgent demand for antifouling coatings in marine industry. Inspired by the unique nanostructure surface of filefish scale, hierarchical films that consist of poly(pentafluorophenyl acrylate) free standing micropillars grafted with pH responsive poly(methacrylic acid) nanobrushes are fabricated by anodic aluminum oxide templating method combined with a subsequent post-polymerization modification strategy. The obtained films exhibit constantly underwater superoleophobicity, furthermore, a pH sensitive functionality, which enables reversible switching between low and high oil adhesion as a result of the adjustable oil sliding angle. This particular study provides a very mild method for the facile fabrication of bioinspired nanostructures with excellent oil-repellent performance and switchable oil-adhesion properties, thus paving the way toward novel functional materials with smart structures for promising applications, such as smart microfluidics, controllable bioadhesion, and intelligent materials for oil removal treatment and marine antifouling.

Superoleophobic surfaces display large contact angles (greater than 150°) against organic liquids in aqueous environment are most widely studied in the past decades because of their excellent oil-repellent ability.^[1–3] Such artificial materials have gained more attention recently attributed to their potential applications in the field of droplet manipulation in microfluidics,^[4] antioil contamination,^[5] resistance reduction of oil transportation,^[6] anti-biofouling,^[7] industrial metal cleaning,^[8] and oil/water separation.^[9] In order to obtain surfaces with more

sophisticated oil-repellent abilities, further development and exploration of new materials and ingenious fabrication methods is necessary. Nature is well versed in creation of surfaces with versatile wettability by managing chemical compositions and surface topography.^[10,11] One of the most common biological surface featuring excellent superoleophobic properties in water is fish scale. Specially, like filefish scales, the binary cooperation of a hydrophilic chemical composition (i.e., collagen) and fine-scaled rough microstructures (i.e., oriented micropapillae with length of 100–300 μm and width of 30–40 μm) distributed on the surface leads to underwater superoleophobicity and antioil ability of scales.^[12,13] By mimicking nanostructured fish scale, Takahara's group has, for example, prepared an underwater superoleophobic surface on poly(methyl methacrylate-co-N-(3,4-dihydroxyphenyl)


methacrylamide) substrate via layer-by-layer assembly of poly(acrylic acid) and poly(ethylene imine).^[14]

To evaluate the performance of superoleophobic materials, oil contact angle (CA) is a key factor. In order to be able to critically evaluate superoleophobic materials, the oil-adhesion ability on the surfaces should be considered. On superoleophobic surfaces with ultralow oil adhesion, an oil droplet can move easily on the surface upon slight titling or shaking; however, on superoleophobic materials with ultrahigh oil-adhesion properties, the oil droplet sticks on the surfaces, rendering such surfaces useful for nonloss oil transportation, which shows great application potential in the field of bioadhesion, or microfluidic technology.^[15–17] As a result, the application range of the underwater superoleophobic materials can be expanded if the oil-adhesion ability of their surfaces is switchable. This seemingly contradictory proposal can be realized with the aid of stimuli responsive materials. Presently, multifunctional superoleophobic surfaces with tunable oil adhesion under external stimulus via photoirradiation,^[18] thermal,^[19] pH,^[20] electric field,^[21] magnetic field^[22] treatment, and multistimulus combinations,^[23] have been discovered by means of electrochemical deposition,^[24] laser ablation,^[25] self-assembly,^[26] chemical etching,^[27] spray/dip coating,^[1] the template method,^[28] lithography,^[29] electrochemical anodization,^[30] and the hydrothermal method^[31] among others.^[13]

Among the numerous methods, templating approach is particularly interesting for the growth of nanostructures and is an ideal procedure for mimicking biological surfaces.^[32–35]

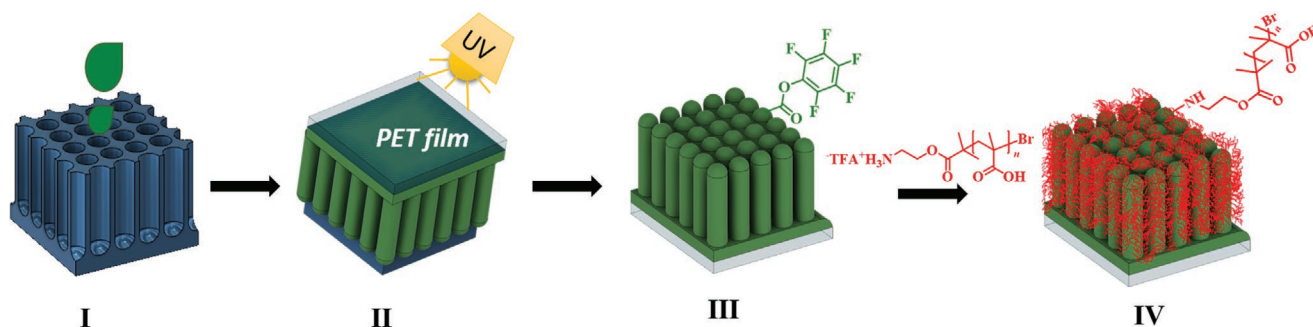
X. Huang, Prof. P. Theato
 Institute for Chemical Technology and Polymer Chemistry (ITCP)
 Karlsruhe Institute of Technology (KIT)
 Engesserstr.18, Karlsruhe D-76131, Germany
 E-mail: patrick.theato@kit.edu

X. Huang, Dr. H. Mutlu, Prof. P. Theato
 Soft Matter Laboratory
 Institute for Biological Interfaces III (IBG 3)
 Karlsruhe Institute of Technology (KIT)
 Herrmann-von-Helmholtz-Platz 1, Eggenstein-Leopoldshafen D-76344,
 Germany

 The ORCID identification number(s) for the author(s) of this article can be found under <https://doi.org/10.1002/admi.202000101>.

© 2020 The Authors. Published by WILEY-VCH Verlag GmbH & Co. KGaA, Weinheim. This is an open access article under the terms of the Creative Commons Attribution-NonCommercial License, which permits use, distribution and reproduction in any medium, provided the original work is properly cited and is not used for commercial purposes.

DOI: 10.1002/admi.202000101



Scheme 1. Schematic illustration of fabrication procedures. I) Drop casting the precursor liquid onto beforehand AAO template. II) UV initiated polymerization in nanopores. III) Dissolution of AAO template and release of pillar-PPFPA texture free stand on the substrate of PET. IV) Grafting of PMAA nanobrushes onto pillar-PPFPA via post-polymerization modification.

Compared to other typical nanoporous templates, anodic aluminum oxide (AAO) membranes have received much attention because of their excellent thermal and chemical stability as well as structural parameters controllability.^[36,37] AAOs with a high areal density (up to 10^{11} cm^{-2} pores) and narrow pore-size distribution over a large area have been applied in various fields, including energy storage and conversion,^[38] sensors,^[39] optical devices,^[40] molecular separation,^[41–43] catalysis,^[44] tissue engineering,^[45] drug delivery,^[46] as well as other applications and aspects.^[47–50] Additionally, the precise controlled arrangement of chemical and structural features of a replica are of particular importance for a nanostructured surface. Until now, many other fabrication methods are synergistic with AAO templating and have been employed for the preparation of nanostructures bearing hierarchical surfaces, however, limitations and drawbacks also emerged.^[10,51–53] Particularly, a complicated post-processing based on AAO template is inevitable, limiting the options of methods, such as surface initiated atom transfer radical polymerization with strict experimental conditions and special requirements of monomers, narrowing down potential applications.^[54]

In order to simplify the fabrication process and broaden the applicability of the AAO template method, post-polymerization modification of the templated polymer structure has been proposed, which is a powerful tool for polymer chemists to prepare highly functionalized macromolecular structures, and hence ideal for the fabrication of smart surfaces from reactive precursor polymers eliminating a complicated polymerization synthesis.^[55–57] In previous studies, we presented that polymers decorated with pentafluorophenyl (PFP) esters are promising active precursors for a post-polymerization modification, because they can react with amines under very mild reaction conditions yielding functionalized polymer architectures, which would not be accessible otherwise.^[58,59] Thus, we are particularly interested in constructing smart surfaces via an AAO template method combining with a post-polymerization modification strategy under mild condition. In this work, active ester bearing poly(pentafluorophenyl acrylate) (PPFPA) micropillars are fabricated by in situ polymerization inside a porous AAO template onto a poly(ethylene terephthalate) (PET) film substrate. Subsequently, amino end-functionalized poly(methacrylic acid) (PMAA) brushes were tethered onto the PPFPA pillars via catalyst-free post-polymerization modification at ambient temperature. The hierarchical surfaces that are formed, mimic biological microtextures and exhibit reversible

pH-switchable oil adhesion as well as persistent underwater superoleophobicity with oil contact angles constantly higher than 150° . Therefore, we anticipate that our approach is providing the guidance for the design of underwater superoleophobic surfaces with a reversible oil-adhesion property for particular potential applications in marine environment.

The fabrication procedure of grafted PMAA nanobrushes onto PPFPA pillars (pillar-PPFPA-g-PMAA) surfaces is illustrated in **Scheme 1**. First, a self-standing highly ordered AAO template featuring hexagonal porous structure was obtained from a two-step anodization process.^[36] Subsequently, a pore-widening procedure was applied, delivering an AAO template with pore diameter of ≈ 300 nm and a pore length of ≈ 3 μm . The corresponding scanning electron microscopy (SEM) images of cross-sectional and top view, respectively, are depicted in Figure S5A,B in the Supporting Information. Pillar-PPFPA were fabricated by replicating the porous structure of the as-prepared AAO template. To do so, PFP monomer solution was infiltrated onto an AAO membrane and then covered with PET film, followed by a photoinitiated polymerization. The AAO template was then dissolved in acidic solution to release active PPFPA pillars. According to SEM results (**Figure 1A,B**), those PPFPA pillars are with identical contour as the prepared AAO template, hence manifesting the successful fabrication of PPFPA pillars via a templating approach. Afterward, amino end-functionalized PMAA polymer chains were grafted onto the PPFPA pillars through active ester-amine chemistry at ambient temperature in DMSO.^[60] Upon conducting the post-polymerization modification for 24, 36, and 48 h, respectively, the pillar-PPFPA-g-PMAA films were obtained. The SEM images after modification are measured and illustrated in Figure 1C,D, depicting that the pillar structure remained free-standing on the PET substrate. As a result, the morphology and state of polymer pillars maintained the same before and after post-polymerization modification, demonstrating the power of the mild post-polymerization modification technique. However, the wettability of the pillar-PPFPA and pillar-PPFPA-g-PMAA grafted surfaces were diacritical from the inserted figures of the surface water contact angle (**Figure 1**). Specifically, the pillar-PPFPA surfaces are inherently hydrophobic with a static water contact angle of $124^\circ \pm 4^\circ$, depicting nonwetting properties with an elliptical geometry of the droplet. Contrastively, a water droplet spread within 3 s with a final contact angle of $20^\circ \pm 3^\circ$ on pillar-PPFPA-g-PMAA surfaces. Hence, after grafting PMAA

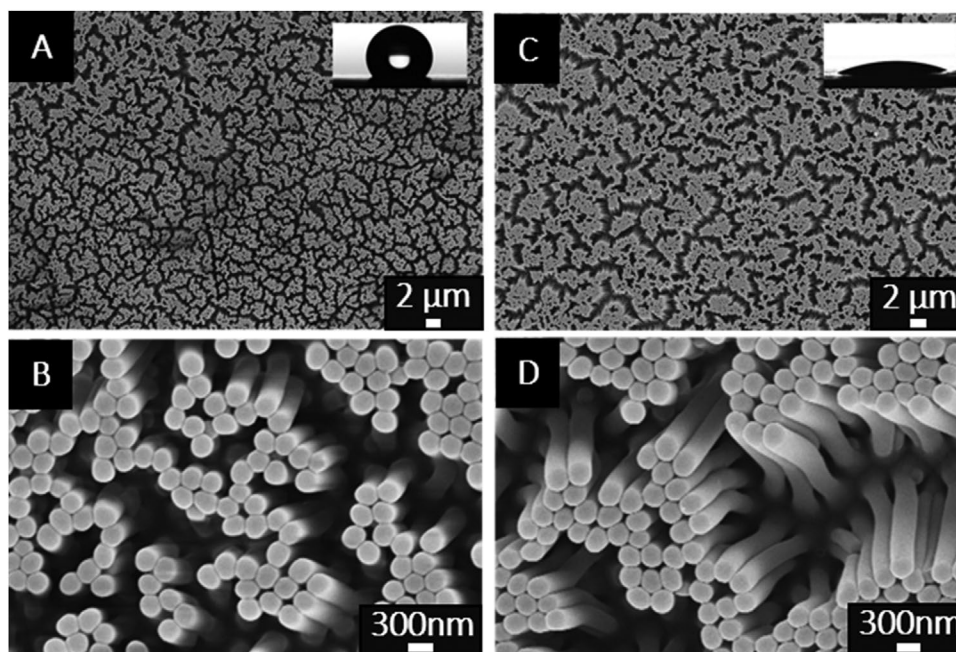


Figure 1. FE-SEM and magnified images of: A,B) PPFPA micropillars; C,D) PPFPA-g-PMAA, and inserted images of water contact angle (WCA) measurements. (Water droplet: 2 μ L.)

brushes onto PPFPA pillar, the hierarchical surface changed from hydrophobic to hydrophilic owing to the introduction of hydrophilic PMAA brushes through the post-polymerization modification.

To further shed light on the efficiency of post-polymerization modification, complementary Fourier-transform infrared spectroscopy (FT-IR) measurements were performed at different reaction time intervals. As demonstrated in **Figure 2**, C=O group of PPFPA micropillars exhibits characteristic bands at 1784 cm^{-1} (marked in blue) and 1517 cm^{-1} (marked in green).

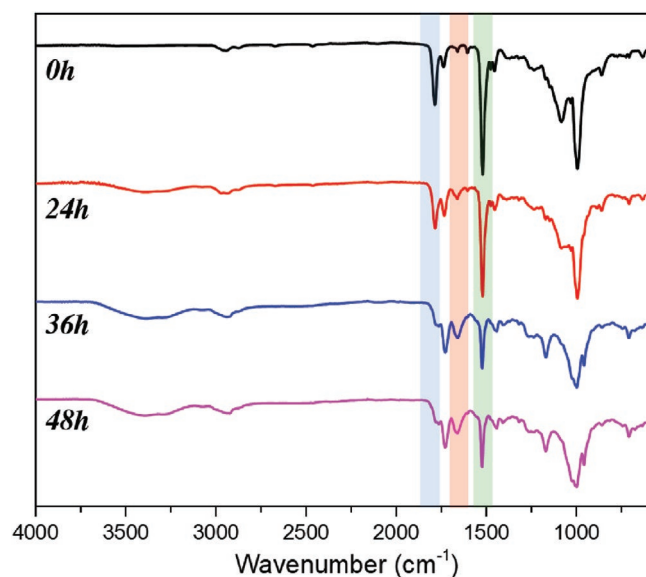


Figure 2. FT-IR spectra of pillar-PPFPA-g-PMAA via post-polymerization modification at different reaction time intervals.

Upon post-polymerization modification, the bands resulted from PPFPA decreased significantly, while a new carbonyl stretching band at 1724 cm^{-1} (marked in red), relevant to the newly formed PMAA brush, increased over time.^[61] After 36 h, the post-polymerization modification reached an end, as the intensity of the bands remained constant even for a prolonged reaction time of 48 h. Nevertheless, the carbonyl stretching vibrations of PFP ester remained with lower intensity even after a 36 h reaction period, attributing to the crosslinked structure of micropillars, which hindered quantitative conversion of amino end-functionalized polymer chains inside the pillars. Notably, it is the surface that has a prominent effect on targeted superoleophobicity and oil-adhesion properties.

The pH-induced swelling and collapse of surface-tethered weak polyelectrolyte brushes (such as PMAA at a $\text{p}K_a = 4.8$) is not only crucial for a fundamental understanding, but also relevant for various practical applications.^[62] For instance, at pH lower than the critical $\text{p}K_a$ value, PMAA with pendant carboxylic acid groups protonated and coiled up forming intermolecular hydrogen bonds, while stretched chains and exclusively formed hydrogen bonds with surrounding water molecules at a high pH value (higher than $\text{p}K_a$), resulting in a pH-induced transformation of the molecular roughness of the surface.^[63] Accordingly, the oil wettability of flat-PPFPA-g-PMAA surfaces changed from $125^\circ \pm 2^\circ$ to $164^\circ \pm 1^\circ$ as the pH value increases, as illustrated in Figure S8 in the Supporting Information. However, the underwater oil contact angle of pillar-PPFPA-g-PMAA surface remained constant, in spite of pH value of the surrounding media has gradually changed from pH = 3 to 11, demonstrating the pillar-PPFPA-g-PMAA surface maintained superoleophobicity at any pH media regarding its hierarchical structuring (**Figure 3**). Indeed, when pillar-PPFPA-g-PMAA is immersed in water, the pillars tend to be freely standing on

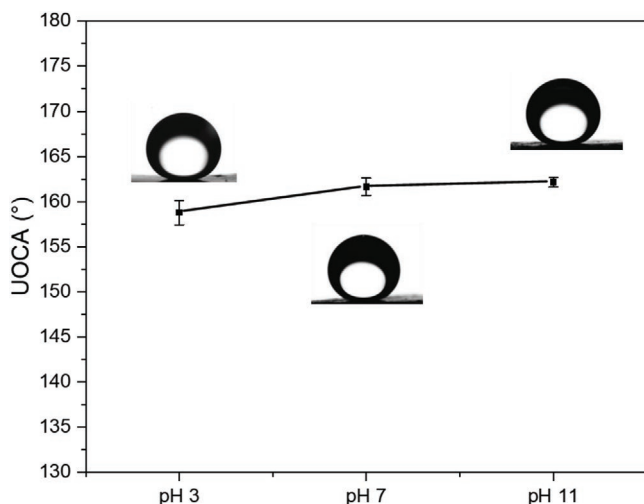


Figure 3. Underwater oil contact angle (UOCA) values and corresponding images of pillar-PPFPA-g-PMAA surface at different pH values. (Oil droplet: 15 μ L.)

the surface. Simultaneously, the trapped water resulting from high degree of surface roughness contributes to the transition of Wenzel to Cassie state of oil droplet underwater. Hence, the films are depicting constant superoleophobicity.^[64]

Within the examined pH range, the oil contact angle kept unchanged, while the oil-adhesion property dramatically altered, as illustrated in **Figure 4A** and the video footage in the Supporting Information, respectively. Indeed, under acidic conditions (pH = 3), the oil droplet adhered strongly to the hierarchical surface and did not slide off, even when the tilting angle reached 45°. When the pH value was lower than the pK_a of PMAA, the brushes tend to collapse and dehydrate, thus generating stronger interaction and larger contact area between the surface and oil droplet. The oil droplet adhering to the grooves of the rough surface formed an underwater Wenzel state, showing a high oil adhesion (schematic illustrated in **Figure 4B**).^[13] However, when the pH value was increased above

pK_a of PMAA and reached to 7, the oil droplet slid off already at a tilting angle of 8°, and with further increase of the pH value to 11, the sliding angle decreased to 3°, demonstrating the opportunity to tune the oil adhesion by varying the pH value. The phenomena can presumably be ascribed to the fact that the induced hydration of the PMAA brushes accompanied by stretching of the brushes at pH values higher than the pK_a of PMAA prevented the interaction between the oil droplet and the surface. When the pH value is 7, the PMAA brushes are partially stretched, the oil droplet thus can partially penetrate into the grooves of the rough surface, revealing an underwater transition state that affords a hysteresis of oil sliding. When further increasing the pH value, full extension of PMAA brushes is obtained and the micro/nanoroughness of the surface tend to be prewetted by water that trapped a water layer underneath the oil droplet. Thus, the pillar-PPFPA-g-PMAA film formed an underwater “Lotus” state (Cassie state), which results in an ultralow oil adhesion of freely oil sliding property.^[11,28] For comparison, the oil sliding angles of flat-PPFPA-g-PMAA surface were also measured, which are illustrated in **Figure S8B** in the Supporting Information. Intriguingly, the oil droplet was tightly adhered to the flat-PPFPA-g-PMAA, in spite of a tilting angle of 45°. Therefore, the results indicate the importance of pillar structures with grafted nanobrushes to prepare underwater superoleophobic surfaces with a pH switchable oil-adhesion property.

For gaining deeper insight into the reversibility of pH responsive oil-adhesion property, we alternatively tested the oil sliding angle in aqueous solutions with pH values of 3, 7, and 11, respectively, in total for five consecutive cycles. The sample was first immersed into the solution and kept for 1 min to reach equilibrium prior measurement. The results are illustrated in **Figure 5**, elucidating a good reversibility of oil sliding angle. For instance, the oil adhesion declined as the pH increased, hence manifesting the decrease of oil sliding angle. When decreasing the pH value further, the oil droplet was capable to stick onto the pillar-PPFPA-g-PMAA surface. After five measurements, the pillar structure remained on the surface without

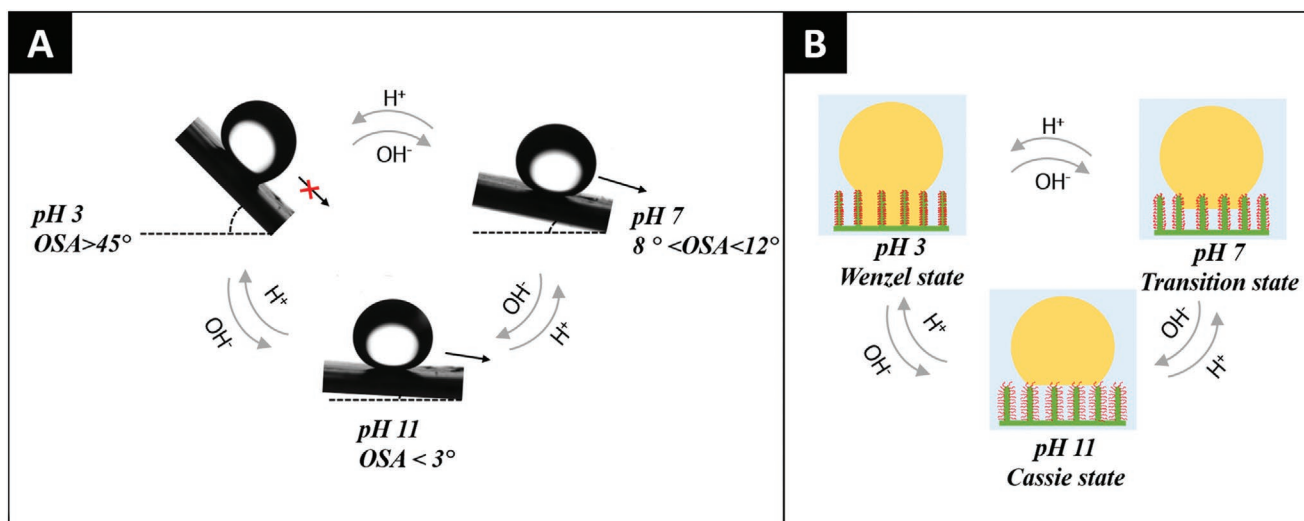


Figure 4. A) Oil sliding angle images of pillar-PPFPA-g-PMAA at different pH conditions. B) Schematic illustration of underwater Wenzel state, transition state, and Cassie state of oil droplet on the pillar-PPFPA-g-PMAA surface.

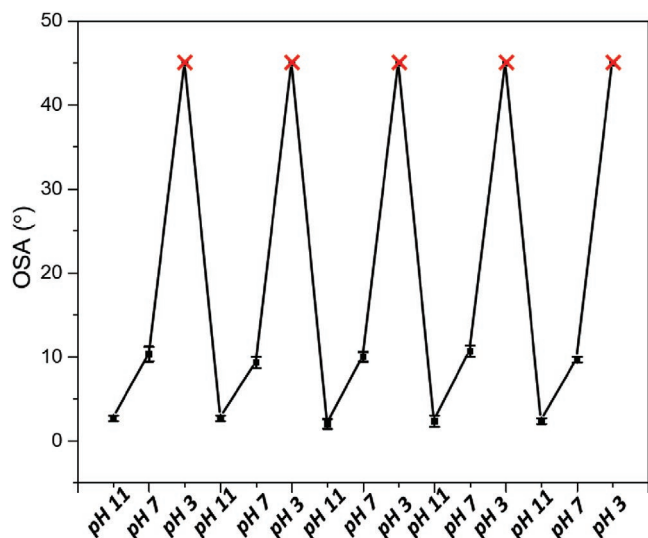


Figure 5. Cycling switchable oil sliding angle (OSA) of pillar-PPFPA-g-PMAA upon pH stimulation.

any damage, as confirmed by SEM measurements (Figure S6, Supporting Information), which demonstrate durability of the functional surface.

In summary, by combining the in situ AAO template polymerization and post-polymerization modification strategy, PPFPA micropillars with grafted PMAA polymer nanobrushes were fabricated, resulting in micro/nanodual hierarchical structural surfaces that revealed tunable oil-adhesion properties while keeping an underwater superoleophobicity. On one hand, an oil droplet can be retained on the surface under acidic conditions and depicting a Wenzel state on the hierarchical surface. While on the other hand, a transition to Cassie state is evolving, i.e., the oil droplet can slide freely on the hierarchical surfaces at neutral and basic pH values. Last but not at least, a pH-stimulated oil sliding property with high reversibility was observed. Correspondingly, we believe that the developed platform paves the way for the fabrication of versatile dynamic surfaces on various substrate by providing a guidance to design of intelligent oil-repellent materials with potential applications varying from smart microfluidics to marine antifouling.

Experimental Section

Materials: Methacrylic acid (MAA) and 1,6-hexanediol diacrylate were obtained from Sigma-Aldrich and purified by passing through a neutral alumina column; 2,2'-azobis(isobutyronitrile) (AIBN, Sigma-Aldrich) was recrystallized from methanol; pentafluorophenyl acrylate (PFPA) and 4-acryloylbzophenone (ABP) were synthesized according to reported procedures.^{165,166} 3-(Trimethoxysilyl)propyl methacrylate was purchased from abcr GmbH; aluminum discs (purity 99.999%) were received from Good Fellow; *N,N,N',N''*-pentamethyldiethylenetriamine (PMDETA), copper(I) bromide (CuBr), 2-hydroxy-4'-(2-hydroxyethoxy)-2-methylpropiophenone (Irgacure 2959), *N*-*boc*-ethanolamine, trimethylamine, 2-bromoisobutyl bromide, trifluoroacetic acid, as well as other general reactants and solvents were purchased from Sigma-Aldrich and used without further purification.

Synthesis of Amine-Functionalized ATRP Initiator *t*-Boc-Aminoethyl 2-Bromoisobutyrate: *N*-*boc*-ethanolamine (1.00 equiv, 3.22 g,

20.00 mmol) and triethylamine (1.20 equiv, 2.43 g, 24.00 mmol) were dissolved in 40 mL of anhydrous dichloromethane (DCM) and cooled in an ice bath. Then, 2-bromoisobutyl bromide (1.06 equiv, 4.87 g, 21.20 mmol) in 10 mL of anhydrous DCM was added dropwise into the mixture. The reaction was slowly warmed up to room temperature and stirred overnight. Then, the precipitate was filtered off, and the filtrate was sequentially washed with saturated sodium bicarbonate solution and deionized water for three times. The organic phase was dried over sodium sulphate and after removing excess DCM under reduced pressure, the crude product was purified by column chromatography over silica gel with DCM/ethyl acetate (v/v, 4:1) as eluent to afford pale yellow liquid. Finally, the *t*-*boc*-aminoethyl 2-bromoisobutyrate was obtained by crystallization in *n*-hexane (−20 °C) as white solid (4.10 g, yield 66%). ¹H NMR (400 MHz, CDCl₃) 4.80 ppm (s, 1H, −NH−), 4.22 ppm (t, 2H, −CH₂OCO−), 3.44 ppm (m, 2H, −NHCH₂−), 1.92 ppm (s, 6H, −C(CH₃)₂Br), 1.43 ppm (s, 9H, −NH*Boc*).

Synthesis of TFA Salt of 2-Aminoethyl 2-Bromoisobutyrate (AEBiBTFA*):** *t*-*Boc*-aminoethyl 2-bromoisobutyrate (4.00 g, 13.00 mmol) was dissolved in 10 mL of trifluoroacetic acid (TFA). After vigorous stirring for 4 h, the excess TFA was removed by rotary evaporation. The obtained solid was processed to recrystallization from diethyl ether, followed by filtration and then dried under vacuum. The collected white solid product was TFA salt of 2-aminoethyl 2-bromoisobutyrate with a yield of 77% (3.20 g). ¹H NMR (400 MHz, CDCl₃) 8.25 ppm (s, 1H, TFA-NH₃⁺CH₂−), 4.48 ppm (t, 2H, −CH₂OCO−), 3.34 ppm (t, 2H, TFA-NH₃⁺CH₂−), 1.94 ppm (s, 6H, −C(CH₃)₂Br).

Synthesis of Amine End-Functionalized PMAA: The typical procedure of atom transfer radical polymerization of methacrylic acid was as follows. 50 μL (2.00 equiv, 0.24 mmol) PMDETA was dissolved in 1 mL deionized (DI) water in Schlenk tube and subjected to a three times freeze–pump–thaw cycle before CuBr (1.00 equiv, 16.90 mg, 0.12 mmol) was added over the frozen solution. In the meantime, MAA (1 mL, 11.80 mmol) was dissolved in 1 mL methanol (MeOH) degassed by three times of freeze–pump–thaw cycles and added into the reaction. Then, AEBiB**TFA* (2.00 equiv, 76.70 mg, 0.24 mmol) was added and freeze–pump–thaw cycles were carried out again three times before being immersed in preheated oil bath at 75 °C to react for 20 h. The reaction was quenched by liquid nitrogen, the final product was precipitated in acetone and dialyzed against MeOH, and then dried under vacuum at 40 °C (yield 45%, 0.50 g). ¹H NMR (400 MHz, DMSO) 12.33 ppm (s, 1H, −CH₂(CH₃)C(COOH)), 1.50–2.05 ppm (m, 2H, −CH₂(CH₃)C(COOH)– the backbone of PMAA), 0.56–1.16 ppm (d, 3H, −CH₂(CH₃)C(COOH)).

Preparation of Anodic Aluminum Oxide Template: AAO templates were prepared using a two-step anodization process.¹⁶⁶ 99.999% pure aluminum discs were mounted in a tetrafluoroethylene case, and then electropolished at 20 V, 5 °C for 6 min in an electrolyte bath mixed with ethanol and perchloric acid (v/v, 3:1) to form a flat surface. Subsequently, the first anodization process was carried out as follows: upon cooling, the electropolished aluminum disks were treated at 1 °C under a voltage of 175 V for 3 h, and then the voltage was increased to 195 V and applied for 20 h. In this process, 1 wt% phosphoric acid (H₃PO₄) was used as electrolyte. After first anodization treatment, irregular layer of aluminum oxide pores were formed and the layer was removed by etching with a mixed aqueous solution of chromic acid (1.80 wt%) and phosphoric acid (6.00 wt%) at 45 °C for 36 h. The aluminum disks were washed thoroughly with deionized water. Next, a second anodization step was proceeded under the voltage of 195 V for 1 h in 1 wt% phosphoric acid at 1 °C. The obtained AAO templates were washed and sonicated with acetone, and dried. A wet chemical etching in 10 wt% H₃PO₄ at 45 °C was applied to AAO template for pore widening for 1 h. Ultimately, all the AAO template was washed and sonicated with acetone, and dried at 45 °C.

Silanization of Poly(ethylene terephthalate) (PET) film: Melinex film was cut into 2.50 × 2.50 cm square sheets and washed with methanol. Then, the sheets were immersed into 4.50 M sodium hydroxide solution at 90 °C for a 2 h hydrolysis. Afterward, the PET sheets were washed with DI water and dried in 45 °C drying oven. Then,

the sheets were processed to a 30 min oxygen plasma treatment and directly immersed into 3-(trimethoxysilyl)propyl methacrylate/toluene (v/v, 1/100) at 90 °C overnight, washed with ethanol thoroughly, and dried before usage.

Preparation of Pillar-PPFPA: Monomer pentafluorophenyl acrylate (1.00 g), photo-crosslinker 4-acryloylbenzophenone (0.05 g), crosslinker 1,6-hexanediol diacrylate (0.05 g), and photoinitiator Irgacure 2959 (0.05 g) were added into 200 μ L of tetrahydrofuran, sealed, and stirred for 1 h until a homogenous solution was obtained. And then, 100 μ L of this monomer solution was dropped onto a prepared AAO template and gently covered with silylated PET film. The sample was then treated under UV (365 nm, 1 W cm^{-2}) for 1 h. Followed by dissolving of the Al layer in CuCl_2/HCl aqueous solution and Al_2O_3 layer in 10 wt% H_3PO_4 solution, the sheet was washed thoroughly with DI water and finally dried under ambient environment.

Post-Polymerization Modification of Pillar-PPFPA with Amine End-Functionalized PMAA: PMAA (0.30 g) polymer was dissolved in 15 mL of DMSO and shaken to form a homogenous solution, into which the PPFPA micropillar film was immersed into and shaken at room temperature for 24, 36, and 48 h, respectively. Afterward, the film was washed thoroughly with ethanol and water, and then dried at room temperature.

Preparation of Flat-PPFPA: The same monomer solution was prepared as for the preparation of pillar-PPFPA surfaces. However, in this case, the monomer solution was spread onto silylated PET film via spin coating with a speed at 1000 rpm s^{-1} for 10 s, and afterward the film was UV polymerized for 1 h, and then washed thoroughly with ethanol and DI water before being dried under ambient temperature.

Post-Polymerization Modification of Pillar-PPFPA with Amine End-Functionalized PMAA: The flat-PPFPA film was immersed into the same PMAA solution in DMSO as illustrated in the post-polymerization modification of pillar-PPFPA and after 36 h, the sample was taken out and rinsed thoroughly with ethanol and water before being dried under ambient temperature.

Instruments and Characterizations—Nuclear Magnetic Resonance (NMR) Spectroscopy: ^1H NMR spectra were conducted on a Bruker Fourier 400 NMR in CDCl_3 and d_6 -DMSO; all chemical shifts were reported in ppm (δ) and calibrated on characteristic solvent signals as internal standards. All data were reported as follows: chemical shift, multiplicity (s = singlet, d = doublet, t = triplet, and m = multiplet).

Instruments and Characterizations—FT-IR: FT-IR spectra were recorded using the attenuated total reflectance infrared spectroscopy (ATR-IR, Smart iTR) unit on a Bruker VERTEX 80 V FT-IR spectrometer in the range of 600–4000 cm^{-1} at ambient temperature.

Instruments and Characterizations—SEM: SEM images were taken with a Zeiss LEO 1530 microscope operating at 5 kV. Samples were sputtered with gold (thickness 5 nm) prior measurement.

Instruments and Characterizations—CA Measurements: The water and oil contact angles were measured using a drop shape analyzer model DSA25S. And, the oil sliding angle was obtained by measuring the contact angle with a tilting speed of 1° s^{-1} , and owing to the limitation of sample water tank, the maximum tilting angle of model test was 45°. 1,2-dichloroethane was used as oil in this study. The pH value was adjusted by 0.1 M HCl and NaOH aqueous solution.

Supporting Information

Supporting Information is available from the Wiley Online Library or from the author.

Acknowledgements

X.H. gratefully acknowledges the China Scholarship Council (CSC grants 201506240019) for partial financial support of this work.

Conflict of Interest

The authors declare no conflict of interest.

Keywords

anodic aluminum oxide, pH response, post-polymerization modification, superoleophobic surfaces

Received: January 19, 2020

Revised: February 17, 2020

Published online: March 29, 2020

- [1] J. Yong, F. Chen, Q. Yang, Z. Jiang, X. Hou, *Adv. Mater. Interfaces* **2018**, *5*, 1701370.
- [2] T. Du, S. Ma, X. Pei, S. Wang, F. Zhou, *Small* **2017**, *13*, 1602020.
- [3] T. Jiang, Z. Guo, W. Liu, *J. Mater. Chem. A* **2015**, *3*, 1811.
- [4] J. Tian, D. Kannangara, X. Li, W. Shen, *Lab Chip* **2010**, *10*, 2258.
- [5] S. Gao, J. Sun, P. Liu, F. Zhang, W. Zhang, S. Yuan, J. Li, J. Jin, *Adv. Mater.* **2016**, *28*, 5307.
- [6] X. Yao, J. Gao, Y. Song, L. Jiang, *Adv. Funct. Mater.* **2011**, *21*, 4270.
- [7] S. Krishnan, C. J. Weinman, C. K. Ober, *J. Mater. Chem.* **2008**, *18*, 3405.
- [8] G. Zhang, X. Zhang, Y. Huang, Z. Su, *ACS Appl. Mater. Interfaces* **2013**, *5*, 6400.
- [9] Z. Xue, S. Wang, L. Lin, L. Chen, M. Liu, L. Feng, L. Jiang, *Adv. Mater.* **2011**, *23*, 4270.
- [10] D. Brodoceanu, C. T. Bauer, E. Kroner, E. Arzt, T. Kraus, *Bioinspiration Biomimetics* **2016**, *11*, 051001.
- [11] B. Su, Y. Tian, L. Jiang, *J. Am. Chem. Soc.* **2016**, *138*, 1727.
- [12] Y. Cai, L. Lin, Z. Xue, M. Liu, S. Wang, L. Jiang, *Adv. Funct. Mater.* **2014**, *24*, 809.
- [13] J. Yong, F. Chen, Q. Yang, J. Huo, X. Hou, *Chem. Soc. Rev.* **2017**, *46*, 4168.
- [14] W. Ma, H. Xu, A. Takahara, *Adv. Mater. Interfaces* **2014**, *1*, 1300092.
- [15] W. Liu, X. Liu, J. Fangteng, S. Wang, L. Fang, H. Shen, S. Xiang, H. Sun, B. Yang, *Nanoscale* **2014**, *6*, 13845.
- [16] X. Liu, J. Zhou, Z. Xue, J. Gao, J. Meng, S. Wang, L. Jiang, *Adv. Mater.* **2012**, *24*, 3401.
- [17] D. Wu, S. Wu, Q. D. Chen, S. Zhao, H. Zhang, J. Jiao, J. A. Piersol, J. N. Wang, H.-B. Sun, L. Jiang, *Lab Chip* **2011**, *11*, 3873.
- [18] D. Tian, Z. Guo, Y. Wang, W. Li, X. Zhang, J. Zhai, L. Jiang, *Adv. Funct. Mater.* **2014**, *24*, 536.
- [19] E. Svetushkina, N. Pureskiy, L. Ionov, M. Stamm, A. Synytska, *Soft Matter* **2011**, *7*, 5691.
- [20] L. D. Zarzar, P. Kim, J. Aizenberg, *Adv. Mater.* **2011**, *23*, 1442.
- [21] A. Pranzetti, S. Mieszkin, P. Iqbal, F. J. Rawson, M. E. Callow, J. A. Callow, P. Koelsch, J. A. Preece, P. M. Mendes, *Adv. Mater.* **2013**, *25*, 2181.
- [22] Z. Cheng, L. Feng, L. Jiang, *Adv. Funct. Mater.* **2008**, *18*, 3219.
- [23] Y. Lai, F. Pan, C. Xu, H. Fuchs, L. Chi, *Adv. Mater.* **2013**, *25*, 1682.
- [24] E. Zhang, Z. Cheng, T. Lv, L. Li, Y. Liu, *Nanoscale* **2015**, *7*, 19293.
- [25] J. Yong, F. Chen, Q. Yang, U. Farooq, H. Bian, G. Du, X. Hou, *Appl. Phys. A* **2015**, *119*, 837.
- [26] Z. Cheng, H. Liu, H. Lai, Y. Du, K. Fu, C. Li, J. Yu, N. Zhang, K. Sun, *ACS Appl. Mater. Interfaces* **2015**, *7*, 20410.
- [27] M. Li, B. Wang, L. Heng, L. Jiang, *Adv. Mater. Interfaces* **2014**, *1*, 1400298.
- [28] T. Du, S. Ma, X. Pei, S. Wang, F. Zhou, *Small* **2017**, *13*, 1602020.
- [29] D. Wu, S. Z. Wu, Q. D. Chen, Y. L. Zhang, J. Yao, X. Yao, L. G. Niu, J. N. Wang, L. Jiang, H. B. Sun, *Adv. Mater.* **2011**, *23*, 545.
- [30] M. Liu, L. Jiang, *Adv. Funct. Mater.* **2010**, *20*, 3753.

- [31] Y. Tokudome, K. Okada, A. Nakahira, M. Takahashi, *J. Mater. Chem. A* **2014**, *2*, 58.
- [32] X. Fan, L. Niu, Z. Xia, *Colloid Polym. Sci.* **2014**, *292*, 3251.
- [33] T. Sakai, Y. Takeoka, T. Seki, R. Yoshida, *Langmuir* **2007**, *23*, 8651.
- [34] X. Zhang, F. Shi, J. Niu, Y. Jiang, Z. Wang, *J. Mater. Chem.* **2008**, *18*, 621.
- [35] L. Sacco, I. Florea, C. S. Cojocaru, *Surf. Coat. Technol.* **2019**, *364*, 248.
- [36] H. Masuda, K. Fukuda, *Science* **1995**, *268*, 1466.
- [37] A. Rath, P. Theato, *Adv. Funct. Mater.* **2020**, *30*, 1902959.
- [38] H. Zhao, M. Zhou, L. Wen, Y. Lei, *Nano Energy* **2015**, *13*, 790.
- [39] E. Park, O. s. Kwon, S. j. Park, J. s. Lee, S. You, J. Jang, *J. Mater. Chem.* **2012**, *22*, 1521.
- [40] D. O'carroll, I. Lieberwirth, G. Redmond, *Nat. Nanotechnol.* **2007**, *2*, 180.
- [41] P. W. Bohn, *Annu. Rev. Anal. Chem.* **2009**, *2*, 279.
- [42] P. Kohli, M. Wirtz, C. R. Martin, *Electroanalysis* **2004**, *16*, 9.
- [43] C. R. Martin, M. Nishizawa, K. Jirage, M. Kang, S. B. Lee, *Adv. Mater.* **2001**, *13*, 1351.
- [44] P. C. Stair, C. Marshall, G. Xiong, H. Feng, M. J. Pellin, J. W. Elam, L. Curtiss, L. Iton, H. Kung, M. Kung, H. H. Wang, *Top. Catal.* **2006**, *39*, 181.
- [45] K. C. Popat, E. E. L. Swan, V. Mukhatyar, K. I. Chatvanichkul, G. K. Mor, C. A. Grimes, T. A. Desai, *Biomaterials* **2005**, *26*, 4516.
- [46] S. Simovic, D. Losic, K. Vasilev, *Chem. Commun.* **2010**, *46*, 1317.
- [47] S. D. Alvarez, C. P. Li, C. E. Chiang, I. K. Schuller, M. J. Sailor, *ACS Nano* **2009**, *3*, 3301.
- [48] M. Wang, G. Meng, Q. Huang, M. Li, Z. Li, C. Tang, *Analyst* **2011**, *136*, 278.
- [49] J. Bachmann, J. Escrig, K. Pitzschel, J. M. M. Moreno, J. Jing, D. Görlitz, D. Altbir, K. Nielsch, *J. Appl. Phys.* **2009**, *105*, 07B521.
- [50] W. C. Tsai, S. J. Wang, J. K. Lin, C. L. Chang, R. M. Ko, *Electrochem. Commun.* **2009**, *11*, 660.
- [51] S. H. Hong, B. J. Bae, H. Lee, J. H. Jeong, *Microelectron. Eng.* **2010**, *87*, 2081.
- [52] K. Liu, J. Du, J. Wu, L. Jiang, *Nanoscale* **2012**, *4*, 768.
- [53] H. Jo, N. Haberkorn, J. A. Pan, M. Vakili, K. Nielsch, P. Theato, *Langmuir* **2016**, *32*, 6437.
- [54] H. Wu, Y. Higaki, A. Takahara, *Prog. Polym. Sci.* **2018**, *77*, 95.
- [55] H. Zhao, P. Theato, *Polym. Chem.* **2013**, *4*, 891.
- [56] P. Theato, *J. Polym. Sci., Part A: Polym. Chem.* **2008**, *46*, 6677.
- [57] S. Lin, A. Das, P. Theato, *Polym. Chem.* **2017**, *8*, 1206.
- [58] N. Haberkorn, K. Nilles, P. Schattling, P. Theato, *Polym. Chem.* **2011**, *2*, 645.
- [59] S. Lin, X. Huang, R. Guo, S. Chen, J. Lan, P. Theato, *J. Polym. Sci., Part A: Polym. Chem.* **2019**, *57*, 1580.
- [60] A. Das, P. Theato, *Chem. Rev.* **2016**, *116*, 1434.
- [61] S. Lin, J. Shang, P. Theato, *ACS Macro Lett.* **2018**, *7*, 431.
- [62] R. L. Gustafson, J. A. Lirio, *J. Phys. Chem.* **1965**, *69*, 2849.
- [63] Q. Cheng, M. Li, F. Yang, M. Liu, L. Li, S. Wang, L. Jiang, *Soft Matter* **2012**, *8*, 6740.
- [64] L. P. Xu, J. Peng, Y. Liu, Y. Wen, X. Zhang, L. Jiang, S. Wang, *ACS Nano* **2013**, *7*, 5077.
- [65] J. Shang, S. Lin, P. Theato, *Polym. Chem.* **2017**, *8*, 7446.
- [66] M. Eberhardt, R. Mruk, R. Zentel, P. Théato, *Eur. Polym. J.* **2005**, *41*, 1569.